Thermal effects on the moment of inertia and gravitational redshift of PSR J1012+5307: implications for hyperonic matter under *SU*(3) and *SU*(6) symmetries*

Y. Xu (许妍)[1,4†] X. L. Huang (黄修林)[1] Y. B. Wang (王夷博)[1] Q. Yuan (袁琦)[1]
W. B. Ding (丁文波)[2] N. An (安宁)[1] Y. F. Shen (申淯夫)[1‡] Z. Yu (喻孜)[3§]

[1]Changchun Observatory, National Astronomical Observatories, Chinese Academy of Sciences, Changchun 130117, China
[2]College of Physics and Electronic Information Engineering, Guangxi Minzu Normal University, Chongzuo 532200, China
[3]College of Science, Nanjing Forestry University, Nanjing 210037, China
[4]School of Astronomy and Space Science, University of Chinese Academy of Sciences, Beijing 100049, China

Abstract: The temperature dependence of neutron star structure significantly alters the equation of state, thereby affecting observable properties such as the moment of inertia and gravitational redshift. Using relativistic mean-field (RMF) theory with hyperonic degrees of freedom under *SU*(3) flavor and *SU*(6) spin-flavor symmetries, we investigate thermal effects on the structural properties of protoneutron stars (PNSs) and cold neutron stars (CNSs). Focusing on PSR J1012+5307, we analyze the pronounced structural transformations that occur during the transition from a PNS to a CNS. For a 1.94 $M_\odot$ hyperonic star under *SU*(3) flavor symmetry, decreasing the temperature from $T = 30$ MeV to 0 MeV induces a radius contraction of approximately 50%, accompanied by a decrease in the moment of inertia of nearly 26% and a substantial increase in gravitational redshift of approximately 154%. Furthermore, we examine variations in the moment of inertia and gravitational redshift arising from the mass uncertainties of PSR J1012+5307. Taking *SU*(3) flavor symmetry at $T = 20$ MeV as an example, increasing the mass across the range 1.72−1.94 $M_\odot$ leads to a radius contraction of 2.749 km, an ~8% increase in the moment of inertia, and a substantial ~40% increase in the gravitational redshift. We find that, in the cold regime and at fixed mass, the radius, moment of inertia, and gravitational redshift of hyperonic matter under *SU*(3) flavor symmetry differ only marginally from those of purely nucleonic matter. This makes it difficult to observationally confirm the presence of hyperons in the core of PSR J1012+5307. Moreover, future observations that can precisely constrain pulsar masses, ideally through long-term monitoring from birth, may help determine more conclusively whether hyperons or other exotic matter reside in individual pulsars.

Keywords: hyperons, proto-neutron stars, relativistic mean field theory, moment of inertia, gravitational redshift

DOI: 10.1088/1674-1137/ae92f5 **CSTR:** 32044.14.ChinesePhysicsC.50114106

I. INTRODUCTION

A protoneutron star (PNS) is a short-lived compact object formed during the core collapse and subsequent supernova explosion of a massive star at a late evolutionary stage. As a crucial evolutionary phase linking supernova outbursts and cold neutron stars (CNSs), the internal structure and dynamical evolution of PNSs directly determine the propagation and revival of supernova shocks and regulate heavy-element nucleosynthesis, as well as the time-dependent characteristics of neutrino spectra [1]. Moreover, the rotational evolution, magnetic field topology, and gravitational deformation of PNSs are important physical origins of supernova gravitational-wave radiation, the central engines of short gamma-ray bursts, and the evolution of binary compact-star mergers [2–6]. Consequently, PNSs play an indispensable role throughout compact-star evolution.

The interior of a PNS is characterized by extreme physical conditions, including ultrahigh density, ul-

Received 26 June 2026; Accepted 30 July 2026

* This work was supported by the Development Project of Science and Technology of Jilin Province (20250102012JC), the Astrometric Reference Frame project (JZZX-04), the National Natural Science Foundation of China (12465023)

† E-mail: xuy@cho.ac.cn
‡ E-mail: shenyf@cho.ac.cn
§ E-mail: ziyu_njfu@163.com

©2026 Chinese Physical Society and the Institute of High Energy Physics of the Chinese Academy of Sciences and the Institute of Modern Physics of the Chinese Academy of Sciences and IOP Publishing Ltd. All rights, including for text and data mining, AI training, and similar technologies, are reserved.

trahigh temperature, strong gravitational fields, and efficient neutrino trapping. These environments far exceed the reproducible conditions of terrestrial laboratories, making PNSs natural cosmic laboratories for investigating fundamental physical problems such as the equation of state (EOS) of hot and dense nuclear matter, the dynamics of strong interactions, superfluid/superconducting behavior, and quark-matter phase transitions [7−9]. The EOS describes the constitutive relationship among the pressure, density, temperature, and composition of dense matter and serves as the key input determining the structure and evolutionary behavior of PNSs [10−22]. Different nuclear-matter models, symmetry-energy parameters, hyperon coupling strengths, and the inclusion or exclusion of quark degrees of freedom can lead to significant variations in the EOS. These differences further affect the mass–radius relation, maximum stable mass, critical rotation frequency, and neutrino-radiation characteristics of PNSs [10, 12, 15−17]. Therefore, systematic investigations of the PNS EOS not only provide strong constraints on the properties of nuclear matter under extreme conditions and critical benchmarks for testing and refining existing nuclear-physics models, but also facilitate the precise characterization of the macroscopic physical properties of PNSs. This, in turn, provides reliable theoretical support for deepening our understanding of supernova explosion mechanisms and advancing frontier observations in gravitational-wave detection, neutrino astronomy, and time-domain surveys [23−27].

However, systematic studies remain lacking on how PNS matter containing a substantial fraction of hyperons can support the evolution of intermediate-mass or massive pulsars, such as PSR J1012+5307, which has a measured mass of $1.83\pm0.11 M_{\odot}$ [28−30]. In this work, we employ relativistic mean field theory (RMFT) to investigate the moment of inertia and gravitational redshift of the PNS associated with PSR J1012+5307. The calculations are performed for matter including hyperons (npH matter), using the GM1 parameter set and incorporating $SU(3)$ flavor and $SU(6)$ spin-flavor symmetries. We aim to analyze the effects of temperature on the moment of inertia and gravitational redshift of PSR J1012+5307, with particular emphasis on the observational signatures arising from the PNS-to-CNS transition. This study seeks to constrain the EOS under extreme conditions and to explore the feasibility of probing exotic matter through future astrophysical observations.

The remainder of this work is organized as follows. In Section II, we describe the finite-temperature, hyperon-included EOS for PNSs constructed within the RMFT framework and present the formalism for calculating the stellar mass, moment of inertia, and gravitational redshift. Section III presents a detailed investigation of the moment of inertia and gravitational redshift of PNSs. Using the GM1 parameter set within the RMFT framework, we study the effects of temperature on these properties for PSR J1012+5307 under both $SU(3)$ flavor and $SU(6)$ spin-flavor symmetries. Section IV summarizes the main results.

II. THEORETICAL FRAMEWORK

A. The EOS of PNS in the RMFT

Within the RMFT framework, PNS matter is described by the following Lagrangian density [15, 18, 20−22]:

$$\begin{aligned}\mathcal{L}=&\sum_{B}\bar{\Psi}_{B}\left(\mathrm{i}\gamma_{\mu}\partial^{\mu}-m_{B}-g_{\omega B}\gamma_{\mu}\omega^{\mu}-g_{\phi B}\gamma_{\mu}\phi^{\mu}-g_{\rho B}\gamma_{\mu}\boldsymbol{\rho}^{\mu}\cdot\boldsymbol{I}_{B}\right.\\&\left.+g_{\sigma B}\sigma+g_{\sigma^{*}B}\sigma^{*}\right)\Psi_{B}+\sum_{l=e}\bar{\Psi}_{l}(i\gamma_{\mu}\partial^{\mu}-m_{l})\Psi_{l}+\frac{1}{2}m_{\omega}^{2}\omega_{\mu}\omega^{\mu}\\&+\frac{1}{2}m_{\phi}^{2}\phi_{\mu}\phi^{\mu}+\frac{1}{2}m_{\rho}^{2}\boldsymbol{\rho}_{\mu}\cdot\boldsymbol{\rho}^{\mu}-\frac{1}{3}a\sigma^{3}-\frac{1}{4}b\sigma^{4}+\frac{1}{2}(\partial_{\nu}\sigma^{*}\partial^{\nu}\sigma^{*}\\&-m_{\sigma^{*}}^{2}\sigma^{*2})+\frac{1}{2}(\partial_{\mu}\sigma\partial^{\mu}\sigma-m_{\sigma}^{2}\sigma^{2})+\frac{1}{4}c_{3}(\omega_{\mu}\omega^{\mu})^{2}-\frac{1}{4}W^{\mu\nu}W_{\mu\nu}\\&-\frac{1}{4}P^{\mu\nu}P_{\mu\nu}-\frac{1}{4}\boldsymbol{R}^{\mu\nu}\cdot\boldsymbol{R}_{\mu\nu}.\end{aligned}\tag{1}$$

In this context, the baryon octet (p, n, Λ, Σ^{+}, Σ^{0}, Σ^{-}, Ξ^{-}, Ξ^{0}) and the leptons (e, ν_e) are included, and PNS matter composed of these particles is referred to as npH matter. $\psi_{B(l)}$ denotes the Dirac field for baryons (or leptons), and γ_u represents the Dirac matrices. The symbol $\boldsymbol{I}_B$ denotes the baryonic isospin matrix, while $m_B(l)$ corresponds to the mass of the respective baryon (or lepton). The coupling strengths between baryons and vector mesons are characterized by the constants $g_{\omega B}$, $g_{\phi B}$, and $g_{\rho B}$ for the ω, ϕ, and ρ mesons, respectively. Additionally, the field-strength tensors for the three mesons are defined as $W_{\mu\nu}=\partial_{\mu}\omega_{\nu}-\partial_{\nu}\omega_{\mu}$, $P_{\mu\nu}=\partial_{\mu}\phi_{\nu}-\partial_{\nu}\phi_{\mu}$, and $R_{\mu\nu}=\partial_{\mu}\rho_{\nu}-\partial_{\nu}\rho_{\mu}$.

According to statistical physics, the partition function of the grand canonical ensemble is defined as [18, 19, 22]

$$Z=\mathrm{Tr}\left[\mathrm{e}^{-(\hat{H}-\mu_{B,l}\hat{N})/(K_{B}T)}\right].\tag{2}$$

Here, $\hat{H}$ and $\hat{N}$ represent the Hamiltonian and particle number operators, respectively, and K_B denotes the Boltzmann constant. In natural units, $K_B=1$. T is the temperature. $\mu_{B,l}$ denotes the chemical potentials of baryons and leptons, which are related by

$$\mu_{B,l}=\mu_{n}-q_{i}(\mu_{e}-\mu_{\nu e}),\tag{3}$$

The grand thermodynamic potential for nuclear matter with volume V can be derived from the partition func-

tion

$$\Omega_{gtp} = PV = -T\ln Z. \tag{4}$$

Within the RMF framework, for the Lagrangian given in Eq. (1), the Hamiltonian operator is

$$\hat{H} = \int_V \mathrm{d}^3x \left[-\langle L\rangle + \bar{\Psi}\gamma_0 k_0 \Psi\rangle\right] = -\langle L\rangle V + \sum_B \left[\varepsilon_B \hat{N}_B + \overline{\varepsilon_B}\hat{\bar{N}}_B\right]. \tag{5}$$

Substituting Eq. (4) into Eq. (2) yields the particle density $\rho_{B,l} = \frac{T}{V}\frac{\partial \ln Z}{\partial \mu_{B,l}}$, energy density $\varepsilon = \frac{T^2}{V}\frac{\partial \ln Z}{\partial T} + \mu_{B,l}\rho_{B,l}$, pressure $P = \frac{T}{V}\ln Z$, and entropy $S = \frac{1}{V}\left(\frac{\partial \Omega_{gtp}}{\partial T}\right)_{V,\mu}$, respectively.

Taking the natural logarithm of the partition function, the partition functions for baryons and leptons can be expressed as follows:

$$\ln Z_{B,l} = \frac{V}{T}\langle\mathcal{L}\rangle\langle+\rangle \sum_{B,l}\frac{2J_{B,l}+1}{2\pi^2}\int_0^\infty k_{B,l}^2 \mathrm{d}k_{B,l} \times \left\{\ln\left[1+\mathrm{e}^{-(\varepsilon_{B,l}(k_{B,l})-\mu_{B,l})/T}\right]\right\}. \tag{6}$$

Here, $\varepsilon_{B,l}(k_{B,l}) = \sqrt{k_{B,l}^2 + m_{B,l}^{*2}}$ is the thermal excitation energy of baryons and leptons.

Within the RMFT framework, the effective two-body nucleon–nucleon interaction is described by the exchange of meson fields. In this approach, the meson fields are replaced by their expectation values, and the meson masses and coupling constants are treated as free parameters determined by fitting experimental data or established theoretical models. Consequently, the five mean meson fields satisfy the equations of motion.

$$\begin{aligned}
&\sum_B g_{\sigma B}\rho_{SB} = m_\sigma^2\sigma^0 + a(\sigma^0)^2 + b(\sigma^0)^3,\\
&\sum_B g_{\sigma^* B}\rho_{SB} = m_{\sigma^*0}^2\sigma^{*0},\\
&\sum_B g_{\omega B}\rho_B = m_\omega^2\omega^0 + c_3(\omega^0)^3,\\
&\sum_B g_{\rho B}\rho_B I_{3B} = m_\rho^2\rho_3^0,\\
&\sum_B g_{\phi B}\rho_B = m_\phi^2\phi^0.
\end{aligned} \tag{7}$$

Here, ρ_{SB} and ρ_B denote the scalar and vector densities, respectively, associated with baryon B.

$$\begin{aligned}
\rho_{SB} &= \frac{1}{\pi^2}\int_0^\infty \mathrm{d}k k^2 \frac{m_B^*}{\sqrt{k^2+m_B^{*2}}}\left(\frac{1}{1+\exp[(\varepsilon_B(k)-\mu_B)/T]}\right),\\
\rho_B &= \frac{1}{\pi^2}\int_0^\infty \mathrm{d}k k^2 \left(\frac{1}{1+\exp[(\varepsilon_B(k)-\mu_B)/T]}\right).
\end{aligned} \tag{8}$$

Within this framework, the EOS for PNS matter can be expressed as follows; the detailed derivation is provided in Refs. [13−15, 18−21].

$$\begin{aligned}
\varepsilon = {}& \frac{1}{2}m_\sigma^2\sigma^2 + \frac{1}{2}m_{\sigma^*}^2\sigma^{*2} + \frac{1}{2}m_\omega^2\omega_0^2 + \frac{1}{2}m_\phi^2\phi^2 + \frac{1}{2}m_\rho^2\rho_{03}^2\\
&+\frac{1}{3}a\sigma^3 + \frac{1}{4}b\sigma^4 + \frac{3}{4}c_3\omega^4 + \sum_B \frac{2J_B+1}{2\pi^2}\int_0^\infty \sqrt{k_B^2+m_B^{*2}}\\
&(\exp[\frac{\varepsilon_B(k)-\mu_B}{T}]+1)^{-1}k_B^2\mathrm{d}k_B + \sum_l \frac{2J_l+1}{2\pi^2}\int_0^\infty \sqrt{k_l^2+m_l^2}\\
&(\exp[\frac{\varepsilon_l(k)-\mu_l}{T}]+1)^{-1}k_l^2\mathrm{d}k_l,
\end{aligned} \tag{9}$$

$$\begin{aligned}
P = {}& -\frac{1}{2}m_\sigma^2\sigma^2 - \frac{1}{2}m_{\sigma^*}^2\sigma^{*2} + \frac{1}{2}m_\omega^2\omega_0^2 + \frac{1}{2}m_\phi^2\phi^2 + \frac{1}{2}m_\rho^2\rho_{03}^2\\
&-\frac{1}{3}a\sigma^3 - \frac{1}{4}b\sigma^4 + \frac{1}{4}c_3\omega^4 + \frac{1}{3}\sum_B \frac{2J_B+1}{2\pi^2}\int_0^\infty \frac{k_B^4}{\sqrt{k_B^2+m_B^{*2}}}\\
&\left(\exp\left[\frac{\varepsilon_B(k)-\mu_B}{T}\right]+1\right)^{-1}\mathrm{d}k_B + \frac{1}{3}\sum_l \frac{2J_l+1}{2\pi^2}\int_0^\infty\\
&\frac{k_l^4}{\sqrt{k_l^2+m_l^2}}\left(\exp\left[\frac{\varepsilon_l(k)-\mu_l}{T}\right]+1\right)^{-1}\mathrm{d}k_l.
\end{aligned} \tag{10}$$

$J_{B,l}$ denotes the spin quantum number. The effective mass of baryons is

$$m_B^* = m_B - (g_{\sigma B}\sigma + g_{\sigma^* B}\sigma^*). \tag{11}$$

Charge neutrality requires that

$$q_B\rho_B + q_e\rho_e = 0. \tag{12}$$

Here, q_B is the electric charge of baryon B. The lepton fraction $Y_l = (\rho_e + \rho_{\nu e})/\rho_B$ is fixed at 0.4, a standard value adopted in the literature for PNS matter shortly after birth (*e.g.*, [12, 15]). Moreover, because muons do not appear when neutrinos are trapped, $Y_{l\mu} = Y_\mu + Y_{\nu\mu} = 0$.

B. Structure and Global Properties of PNSs: Mass, Radius, Moment of Inertia, and Surface Gravitational Redshift

To compare theoretical models with pulsar observations, macroscopic stellar properties must be computed. Once the EOS is specified, the masses and radii of PNSs can be derived from the Tolman-Oppenheimer-Volkoff

(TOV) equations for hydrostatic equilibrium [31–33]:

$$\begin{aligned}&\frac{\mathrm{d}p}{\mathrm{d}r}=-\frac{(p+\varepsilon)(m+4\pi r^3 p)}{r(r-2m)},\\&m=4\pi\int_0^r \varepsilon r'^2\mathrm{d}r',\\&M=m(R).\end{aligned}\tag{13}$$

The spacetime metric for a slowly rotating PNS in spherical coordinates (t,r,θ,ϕ) is given by [19–21, 34–35]

$$\begin{aligned}\mathrm{d}s^2=&-\mathrm{e}^{2\phi(r)}\mathrm{d}t^2+\left[1-\frac{2m(r)}{r}\right]^{-1}\mathrm{d}r^2\\&-2\omega r^2\sin^2\theta\,\mathrm{d}t\mathrm{d}\phi+r^2(\mathrm{d}\theta^2+\sin^2\theta\mathrm{d}\phi^2).\end{aligned}\tag{14}$$

At leading order, the moment of inertia of a PNS is obtained by

$$I\equiv\frac{J}{\Omega}=\frac{8\pi}{3}\int_0^R(\varepsilon+P)\mathrm{e}^{-\phi(r)}\left[1-\frac{2m(r)}{r}\right]^{-\frac{1}{2}}\frac{\varpi}{\Omega}r^4\mathrm{d}r,\tag{15}$$

where Ω denotes the stellar angular velocity, and ω is the angular velocity measured by a distant observer. The quantity $\varpi=\Omega-\omega$ represents the frame-dragging angular velocity, and the angular velocity of a point within the star, measured by this observer relative to the local inertial frame, is specified by the following equation:

$$\frac{1}{r^4}\frac{\mathrm{d}}{\mathrm{d}r}\left[r^4 j(r)\frac{\mathrm{d}\varpi}{\mathrm{d}r}\right]+\frac{4}{r}\frac{\mathrm{d}j(r)}{\mathrm{d}r}\varpi=0.\tag{16}$$

The metric function $\phi(r)$ is determined by

$$\frac{\mathrm{d}\phi(r)}{\mathrm{d}r}=\frac{m(r)+4\pi r^3 P(r)}{r(r+2m(r))},\tag{17}$$

where

$$j(r)=\begin{cases}\left[1-\dfrac{2m(r)}{r}\right]^{\frac{1}{2}}\mathrm{e}^{-\phi(r)}, & r\leqslant R,\\ 1, & r>R.\end{cases}\tag{18}$$

The gravitational redshift at the PNS surface can be evaluated as [36–37]

$$z=\frac{1}{\sqrt{1-2(M/R)}}-1.\tag{19}$$

The theoretical moment of inertia and surface gravitational redshift of a PNS can be obtained by solving the TOV equations.

C. The RMFT coupling constants

In this work, the GM1 parameter set, which is widely used to describe neutron star properties, is adopted for the nucleon coupling constants in PNS matter. These constants are determined from the saturation properties of nuclear matter, including the saturation density (ρ_B^0), incompressibility coefficient (K_0), binding energy per nucleon (ε_0), symmetry energy (a_4), slope parameter (L), and ratio of the effective nucleon mass to the nucleon mass (m_N^*/m_N) [13–14]. Since the critical density for hyperon onset is significantly higher than the nuclear saturation density, the nucleon–meson coupling constants cannot be extrapolated to the high-density regime. Instead, the hyperon–meson coupling constants in this work are determined using the widely adopted $SU(3)$ flavor and $SU(6)$ spin–flavor symmetries [32, 38–39].

The couplings of the ω, ρ, and ϕ mesons to baryons satisfy the following relations under $SU(3)$ flavor and $SU(6)$ spin–flavor symmetries: $g_{\sigma^*\Sigma}=g_{\sigma^*\Lambda}$, $g_{\omega\Sigma}=g_{\omega\Lambda}$, $g_{\rho\Sigma}=2g_{\rho\Xi}=2g_{\rho N}$, and $g_{\phi\Sigma}=g_{\phi\Lambda}$. Under $SU(3)$ flavor symmetry, they can be obtained from

$$\begin{aligned}&g_{\omega\Lambda}=\frac{g_{\omega N}}{1+\sqrt{3}z\tan\theta_v},g_{\omega\Xi}=\frac{(1-\sqrt{3}z\tan\theta_v)g_{\omega N}}{1+\sqrt{3}z\tan\theta_v},\\&g_{\phi\Lambda}=\frac{-\tan\theta_v g_{\omega N}}{1+\sqrt{3}z\tan\theta_v},g_{\phi\Xi}=-\frac{(\sqrt{3}z+\tan\theta_v)g_{\omega N}}{1+\sqrt{3}z\tan\theta_v}.\end{aligned}\tag{20}$$

Here, $\theta_v=37.5^\circ$ and $z=0.1949$.

Under $SU(6)$ spin–flavor symmetry, they can be obtained from

$$g_{\omega\Lambda}=\frac{2}{3}g_{\omega N},g_{\phi\Lambda}=\frac{1}{2}g_{\phi\Xi}=\frac{\sqrt{2}}{3}g_{\omega N}.\tag{21}$$

Here, $\theta_v\approx35.26^\circ$ and $z=\dfrac{1}{\sqrt{6}}$. The remaining values of the GM1 parameter set are listed in Table 1.

III. ANALYSIS AND DISCUSSION

In this work, we analyze the impact of temperature on the macroscopic properties of PNSs, focusing on the EOSs, mass–radius profiles, mass–energy density relations, and the correlations of moment of inertia and gravitational redshift with mass, radius, and energy density. The analysis is performed at temperatures of $T=20$ and 30 MeV using the RMFT model with the GM1 parameter set under $SU(3)$ flavor and $SU(6)$ spin-flavor symmetries, respectively. Specifically, we consider the intermediate-mass or massive PNS PSR J1012+5307, with a measured mass of $1.83\pm0.11\,M_\odot$, as a representative case to investigate these macroscopic properties within its specific mass range.

Figure 1 illustrates the EOSs of PNSs, along with the mass–radius and mass–energy density relationships. For

Table 1. The GM1 parameter set [38–39].

Saturation properties of nuclear matter									
Quantity	ρ_B^0/fm^{-3}	K_0/MeV	ε_0	a_4/MeV	L/MeV	m_N^*/m_N			
Value	0.153	300	−16.3	32.5	93.9	0.70			
Coupling constants									
Coupling	$g_{\sigma\Lambda}$	$g_{\sigma\Sigma}$	$g_{\sigma\Xi}$	$g_{\sigma^*\Lambda}$	$g_{\sigma^*\Xi}$	$g_{\omega N}$	g_{σ^*N}	$g_{\phi N}$	
Value ($SU6$)	5.84	3.87	3.06	3.73	9.67	10.61	0.00	–	
Value ($SU3$)	7.25	5.28	5.87	2.60	6.82	10.26	0.00	−3.50	
Coupling	$g_{\sigma N}$	$g_{\rho N}$	$g_{\rho\Lambda}$	a (fm^{-1})	b				
Value ($SU6$)	9.57	4.10	0.00	12.28	−8.98				
Value ($SU3$)	9.57	4.10	0.00	12.28	−8.98				
Baryon and meson masses									
Particle	m_σ	m_{σ^*}	m_ω	m_ρ	m_ϕ	m_N	m_Λ	m_Σ	m_Ξ
Mass /MeV	550	975	783	770	1020	939	1116	1193	1318

comparison, the numerical results for CNSs are shown by the solid, dashed, and dotted cyan lines, representing p, n, e, ν_e (npe) matter, npH matter under $SU(3)$ flavor symmetry, and npH matter under $SU(6)$ spin-flavor symmetry, respectively. Finite-temperature EOSs for hyperonic PNS matter at $T = 20$ MeV are shown by the red dashed ($SU(3)$) and dotted ($SU(6)$) lines, while the corresponding results at $T = 30$ MeV are shown by the blue dashed ($SU(3)$) and dotted ($SU(6)$) lines. Red stars denote the maximum-mass values. This notation is used consistently throughout the work.

As shown in Fig. 1(a), the EOSs exhibit a non-monotonic dependence on temperature. Under both $SU(3)$ flavor and $SU(6)$ spin-flavor symmetries, the EOS at $T = 30$ MeV is stiffer than that at $T = 20$ MeV at low energy densities but gradually softens at higher energy densities. For npH matter under $SU(6)$ spin-flavor symmetry, the EOS at $T = 0$ MeV is slightly softer than that at $T = 20/30$ MeV at low energy densities. However, as the energy density increases, it first stiffens progressively before softening considerably, leading to an increasingly pronounced deviation from the finite-temperature PNS curves at intermediate and high energy densities. For npH matter under $SU(3)$ flavor symmetry, the $T = 0$ MeV EOS exhibits behavior similar to that observed under $SU(6)$ spin-flavor symmetry at low densities when compared with the $T = 20/30$ MeV cases. Nevertheless, with increasing energy density, this evolution is notably more moderate than the temperature dependence observed under $SU(6)$ spin-flavor symmetry. This indicates that the distinct variations in meson–baryon coupling strengths between the $SU(3)$ flavor and $SU(6)$ spin-flavor symmetries —particularly the repulsive contribution of the ϕ meson to the nucleon–nucleon interaction (see Table 1)— result in a significantly smaller temperature-induced deviation in the EOS for $SU(3)$ than for $SU(6)$. Furthermore, at a fixed temperature ($T = 0$, 20, or 30 MeV), the EOS of npH matter under $SU(3)$ flavor symmetry remains significantly stiffer than that under $SU(6)$ spin-flavor symmetry in the intermediate- to high-energy-density regime. Notably, the CNS composed solely of npe matter retains the stiffest EOS. Overall, the temperature dependence of the EOSs for hyperonic PNSs remains sufficient to drive substantial changes in macroscopic properties, such as the mass–radius and mass–energy density relations illustrated in Fig. 1(b) and Fig. 1(c). Specifically, as shown in Fig. 1(b) and Fig. 1(c), the radius of a PNS at a fixed mass decreases markedly with decreasing temperature, whereas the central energy density increases, regardless of the symmetry considered. For a fixed radius or energy density, the PNS mass exhibits a significant decreasing trend with decreasing temperature under both $SU(3)$ flavor and $SU(6)$ spin-flavor symmetries. To clearly illustrate the macroscopic properties of maximum-mass stars and PSR J1012+5307, Tables 2 and 3 list the radius, central energy density, moment of inertia, and gravitational redshift for these configurations under both symmetries.

The macroscopic properties of PNSs and CNSs, particularly the moment of inertia (I) and gravitational redshift (z), exhibit distinct structural responses to temperature variations, as illustrated in Figs. 2 and 3. For CNSs ($T = 0$ MeV), I generally increases with mass but declines in the high-mass regime, consistent with standard stellar structure theory. Under both symmetry schemes, I of the PNS initially decreases with increasing mass at $T = 20$ MeV. At higher masses, however, its evolution closely follows that of a CNS. In contrast, at $T = 30$ MeV, I exhibits a monotonic decline across the entire mass range. Conversely, z increases monotonically with mass for both CNSs and PNSs. Moreover, z of the CNS

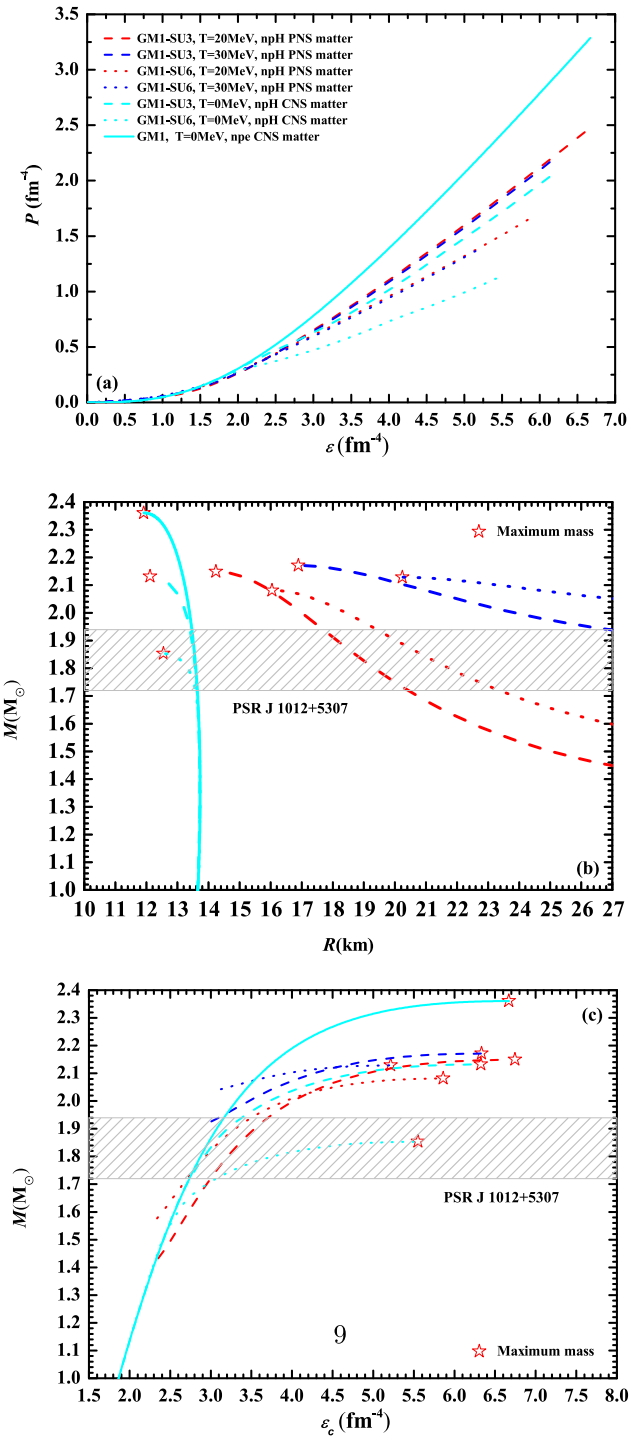


Fig. 1. (color online) (a) EOSs of PNSs and CNSs. (b) Mass-radius relations. (c) Mass-central energy density relations. Cyan lines show the CNS results at $T = 0$ MeV. Solid lines correspond to npe matter, whereas dashed and dotted lines correspond to npeH matter with $SU(3)$ flavor and $SU(6)$ spin-flavor symmetries, respectively. Red and blue lines show the PNS results at $T = 20$ MeV (red) and $T = 30$ MeV (blue) under $SU(3)$ (dashed) and $SU(6)$ (dotted) symmetries, respectively. Red stars indicate the maximum masses for each configuration. This notation is used consistently in subsequent figures.

consistently exceeds that of the PNS at a given mass. Furthermore, I and z of the PNS decrease with decreasing temperature, regardless of whether the radius (R) or the central energy density (ε) is held fixed. For npH matter under $SU(3)$ flavor symmetry, I of the PNS exceeds that of the CNS at $T = 30$ MeV across the entire mass range, whereas at $T = 20$ MeV, I of the PNS is larger than that of the CNS at low and intermediate masses but falls below it at higher masses. This trend is particularly evident for PSR J1012+5307. Based on the numerical results presented in Figs. 2(b) and 2(c), 3(b) and 3(c), and Table 3, we now examine the temperature-driven transition from a PNS to a CNS for hyperonic PSR J1012+5307 under $SU(3)$ flavor symmetry. Taking a 1.94 $M_\odot$ configuration as an example, decreasing the temperature from $T = 30$ to 20 MeV and finally to 0 MeV results in a substantial contraction of R from 26.917 to 17.686 km, ultimately stabilizing at 13.400 km. This contraction is accompanied by an increase in ε from 3.097 to 3.704 fm^{-4} at $T = 20$ MeV, before settling at 3.382 fm^{-4} in the cold phase. Concurrently, I decreases from 3.718×10^{45} to 2.641×10^{45} g·cm^2, eventually recovering slightly to 2.747×10^{45} g·cm^2. In tandem, z increases significantly from 0.127 to 0.216, reaching 0.322 in the cold phase. In addition, for npH matter under $SU(6)$ spin-flavor symmetry, I of the PNS at both $T = 20$ and 30 MeV remains larger than that of the CNS.

If this object is a hot PNS containing hyperons (npH matter), we can examine the variations in I and z arising from mass uncertainties. Taking the $T = 20$ MeV case as an example, under $SU(3)$ flavor symmetry, increasing the mass from 1.72 to 1.94 $M_\odot$ corresponds to a contraction in R from 20.435 to 17.686 km, accompanied by an increase in ε from 2.997 to 3.704 fm^{-4}. Concurrently, I increases from 2.440×10^{45} to 2.641×10^{45} g·cm^2, while z increases from 0.154 to 0.216. Analogous behavior is observed under $SU(6)$ spin–flavor symmetry. Further refinement of the mass measurement of this star would enable more detailed studies to help determine whether hyperons appear in a PNS and identify their specific species. Interestingly, as listed in Table 3, for PSR J1012+5307 at $T = 0$ MeV, the macroscopic properties of npH matter under $SU(3)$ flavor symmetry differ only marginally from those of npe matter. For instance, at a fixed mass of 1.94 $M_\odot$ under $SU(3)$ flavor symmetry, the npH star has $R = 13.400$ km, compared with 13.461 km for the npe star; $\varepsilon = 3.382$ fm^{-4}, compared with 3.163 fm^{-4}; $I = 2.747\times10^{45}$ g·cm^2, compared with 2.774×10^{45} g·cm^2; and $z = 0.322$, compared with 0.319. A similar pattern holds at 1.72 and 1.83 $M_\odot$, where the discrepancies remain similarly small. These marginal differences imply that observationally confirming the presence of hyperons in cold pulsars such as PSR J1012+5307 remains challenging with current data. However, this challenge may be overcome by tracking the evolutionary history. Indeed, if

Table 2. Radii, central energy densities, moments of inertia, and gravitational redshifts of maximum-mass PNSs and CNSs under *SU*(3) flavor and *SU*(6) spin-flavor symmetries.

Parameter (Unit)	T/ MeV	$M_{\max}$ /$M_{\odot}$	R/km	ε_0/fm^{-4}	I/(10^{45} g·cm^2)	z
npeH (*SU*(3))	0	2.132	12.119	6.326	2.613	0.443
	20	2.149	14.241	6.746	2.537	0.343
	30	2.171	16.890	6.334	2.727	0.270
npeH (*SU*(6))	0	1.853	12.549	5.552	2.214	0.332
	20	2.081	16.045	5.862	2.627	0.273
	30	2.129	20.238	5.216	3.065	0.204
npe	0	2.361	11.915	6.671	3.061	0.552

Table 3. Radii, central energy densities, moments of inertia, and gravitational redshifts for CNSs and PNSs in the mass range of PSR J1012+5307, calculated at various temperatures under *SU*(3) flavor and *SU*(6) spin-flavor symmetries.

PSR J-1012+5307	*SU*(3) (*SU*(6))					
	T/MeV	$M/M_{\odot}$	R/km	ε_0/fm^{-4}	I/ (10^{45} g·cm^2)	z
npeH	0	1.72	13.625(13.576)	2.744(3.065)	2.395(2.371)	0.263(0.264)
	0	1.83	13.543(13.099)	2.992(4.277)	2.581(2.386)	0.290(0.305)
	0	1.94	13.400(-)	3.382(-)	2.747(-)	0.322(-)
	20	1.72	20.435(23.375)	2.997(2.708)	2.440(2.820)	0.154(0.130)
	20	1.83	18.966(21.214)	3.296(3.030)	2.538(2.827)	0.183(0.158)
	20	1.94	17.686(19.417)	3.704(3.502)	2.641(2.864)	0.216(0.191)
	30	1.72	-(-)	-(-)	-(-)	-(-)
	30	1.83	-(-)	-(-)	-(-)	-(-)
	30	1.94	26.917(-)	3.097(-)	3.718(-)	0.127(-)
npe	0	1.72	13.636	2.736	2.397	0.262
	0	1.83	13.564	2.930	2.588	0.289
	0	1.94	13.461	3.163	2.774	0.319

future observations can trace the thermal evolution of a pulsar from its birth through the PNS-to-CNS transition, the variations in radius, moment of inertia, and gravitational redshift predicted by our models may provide valuable insights into exotic matter. Although this work focuses on hyperonic EOSs within the RMFT framework using the GM1 parameter set, it provides a foundation for understanding how thermal effects reveal strange particles in neutron stars. Future studies incorporating additional exotic degrees of freedom, such as quark matter, will further refine these constraints.

IV. SUMMARIZES

In summary, this study highlights the crucial role of temperature in determining the macroscopic properties of hyperonic PNSs. We find that the EOS exhibits a non-monotonic temperature dependence, leading to a substantial structural transformation during the transition from a PNS to a CNS. Using the PNS associated with PSR J1012+5307, with a mass of 1.94 $M_{\odot}$ under *SU*(3) flavor symmetry, we demonstrate that the star undergoes substantial contraction as the temperature decreases from $T = 30$ MeV to 0. The radius decreases by approximately 50% (from 26.917 to 13.400 km), accompanied by a reduction in the moment of inertia of nearly 26% (from 3.718×10^{45} to 2.747×10^{45} g·cm^2) and an increase in the gravitational redshift of approximately 154% (from 0.127 to 0.322). To quantify the impact of mass uncertainty on the PNS associated with PSR J1012+5307, we analyze variations in the moment of inertia and gravitational redshift at $T = 20$ MeV. Taking *SU*(3) symmetry as an example, increasing the mass across the range 1.72−1.94 $M_{\odot}$ induces a radius contraction of 2.749 km (from 20.435 to 17.686 km), a ~8% increase in the moment of inertia (from 2.440×10^{45} to 2.641×10^{45} g·cm^2), and a ~40% increase in the gravitational redshift (from 0.154 to 0.216). In addition, our results reveal that the macroscopic properties of npH and npe matter exhibit only minimal variations for PSR J1012+5307 at fixed masses under

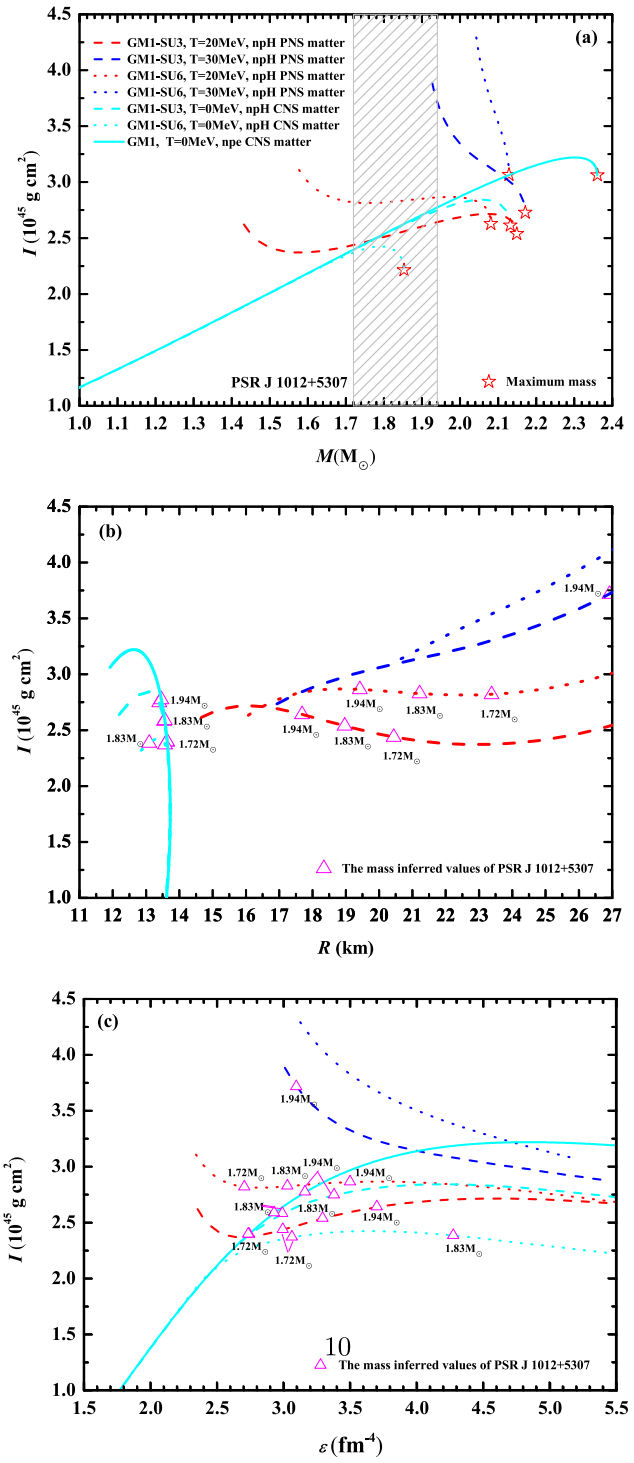


Fig. 2. (color online) Moment of inertia of PNSs and CNSs. (a) Moment of inertia as a function of mass. (b) Moment of inertia as a function of radius. (c) Moment of inertia as a function of central energy density. Pink triangles denote mass measurements of PSR J1012+5307. This notation is used consistently in subsequent figures.

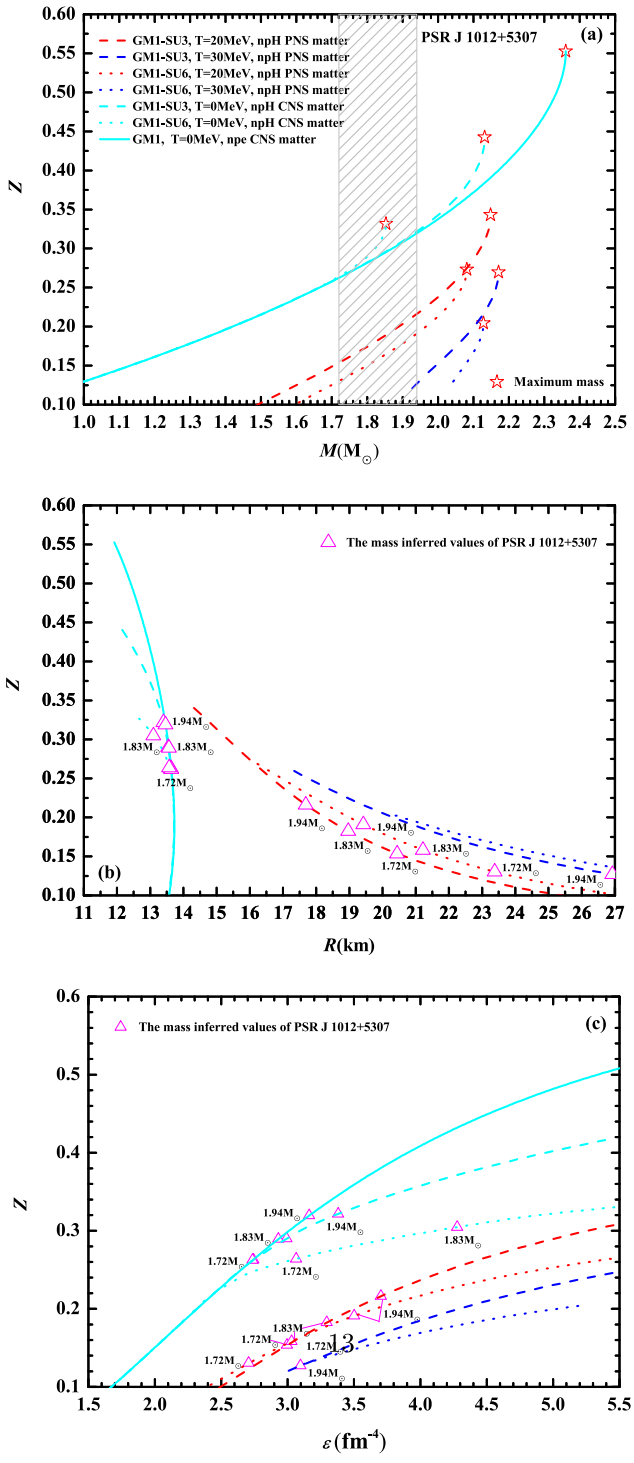


Fig. 3. (color online) Gravitational redshift of PNSs and CNSs. (a) Gravitational redshift as a function of mass. (b) Gravitational redshift as a function of radius. (c) Gravitational redshift as a function of central energy density.

SU(3) flavor symmetry, making it challenging to observationally confirm the presence of hyperons in a CNS. Refining the mass measurement of PSR J1012+5307 through future observations, together with long-term monitoring of a pulsar's evolution from birth, would enable deeper investigation of the emergence of hyperons and the specific types of exotic matter within PNSs.

References

[1] A. Mezzacappa, A. C. Calder, S. W. Bruenn *et al.*, Astrophys. J. **495**, 911 (1998)
[2] V. Ferrari, L. Gualtieri, J. A. Pons *et al.*, Mon. Not. R. Astron. Soc. **350**, 763 (2004)
[3] N. Rea, P. Esposito, R. Turolla *et al.*, Science **330**, 6006 (2010)
[4] S. K.Lander, P. Haensel, B. Haskell *et al.*, Mon. Not. R. Astron. Soc. **503**, 875 (2021)
[5] B. Margalit, A. S. Jermyn, B. D. Metzger *et al.*, Astrophys. J. **939**, 51 (2022)
[6] G. Camelio, A. Lovato, L. Gualtieri *et al.*, Phys. Rev. D **96**, 043015 (2017)
[7] H. Shen, H.Toki, K.Oyamatsu *et al.*, Nucl. Phys. A **637**, 435 (1998)
[8] J. A. Pons, S. Reddy, M. Prakash *et al.*, Astrophys. J. **513**, 780 (1999)
[9] A. Arcones, G. Martínez-Pinedo, E. O'Connor *et al.*, Phys. Rev. C **78**, 015806 (2008)
[10] N. K. Glendenning, S. A. Moszkowski, Phys. Rev. Lett. **67**, 2414 (1991)
[11] J. M. Lattimer, D. F. Swesty, Nucl. Phys. A **535**, 331 (1991)
[12] M. Prakash, I. Bombaci, M.Prakash *et al.*, Phys. Rep. **280**, 1 (1997)
[13] N. K. Glendenning, *Compact stars : nuclear physics, particle physics, and general relativity*, 2nd ed. (New York: Springer, 2000)
[14] I. Bednarek, R. Manka, Phys. Rev. C **73**, 045804 (2006)
[15] Z. Yu, G. Z. Liu, M. F. Zhu *et al.*, Chin. Phys. Lett. **26**, 022601 (2009)
[16] Z. Yu, G. Z. Liu, M. F. Zhu *et al.*, Chin. Phys. C **33**(S1), 70 (2009)
[17] L. F. Roberts, G. Shen, V. Cirigliano *et al.*, Phys. Rev. Lett. **108**, 061103 (2012)
[18] B. Hong, H. Y. Jia, X. L. Mu *et al.*, Chin. Phys. C **40**(6), 065101 (2016)
[19] B. Hong, Z. Z. Ren, Chin. Phys. C **42**(8), 084105 (2018)
[20] X. F. Zhao, B. Tang, Braz. J. Phys. **52**, 149 (2022)
[21] X. F. Zhao, Z. H. Wu, Braz. J. Phys. **53**, 8 (2022)
[22] J. L. Huo, X. H. Wu, W. B. Ding *et al.*, Contrib. Astron. Obs. Skalnaté Pleso **56**, 35 (2026)
[23] H. Y. Duan, A. Friedland, G. C. McLaughlin *et al.*, J. Phys. G: Nucl. Part. Phys. **38**, 035201 (2011)
[24] G. Camelio, L. Gualtieri, J. A. Pons *et al.*, Phys. Rev. D **94**, 024008 (2016)
[25] A. Pascal, J. Novak, M. Oertel *et al.*, Mon. Not. R. Astron. Soc. **511**, 356 (2022)
[26] İ. Bakır, K. Y. Ekşi, Mon. Not. R. Astron. Soc. **546**, stag051 (2026)
[27] B. Müller, arXiv: 2603.24243
[28] J. Antoniadis, T. M. Tauris, F. Ozel *et al.*, arXiv: 1605.01665
[29] D. Mata Sánchez, A. G. Istrate, M. H. van Kerkwijk *et al.*, Mon. Not. R. Astron. Soc. **494**, 4031 (2020)
[30] N. Wei, K. Xu, Z. F. Gao *et al.*, Astrophys. J. **962**, 54 (2024)
[31] R. C. Tolman, Phys. Rev. **55**, 364 (1939)
[32] Y. Xu, Y. F. Shen, Q. Yuan *et al.*, Chin. Phys. C **50**(3), 034108 (2026)
[33] J. R. Oppenheimer and G. M. Volkoff, Phys. Rev. **55**, 374 (1939)
[34] S. Y. Zhao, C. Z. Liu, X. L. Huang *et al.*, Acta Phys. Sin. **70**, 222601 (2021)
[35] X. F. Zhao, Pramana J. Phys. **97**, 209 (2023)
[36] F. Douchin, P. Haensel, Astron. Astrophys. **380**, 151 (2001)
[37] D. L. Benjamin, N. Mohit, and J. O. Benjamin, Phys. Rev. D **73**, 024021 (2006)
[38] T. Miyatsu, M. K. Cheoun, K. Saito, Phys. Rev. C **88**, 015802 (2013)
[39] Y. Xu, B. Diao, Y. B. Wang *et al.*, Res. Astron. Astrophys. **23**, 055016 (2023)